Co, but the hard layer only decayed to 65% of its original remanence when it was coupled to 150 Å $Ni_{40}Fe_{60}$. With a thicker $Co_{75}Pt_{12}Cr_{13}$ hard layer of 150 Å and a $Ni_{40}Fe_{60}$ free layer, the structure was stable to at least 10^7 cycles.

A possible explanation of the decay of the hard layer moment with cycling of the free layer moment is that the decay results from the demagnetizing field at the hard layer that is associated with domain walls in the free layer. The strength of the demagnetizing field will depend on the detailed structure of the domain walls in the free layer. These domain walls are likely to be different in Co and NiFe because of their different anisotropies. Through their associated demagnetizing fields, the motion of the domain walls during the reversal of **M** will demagnetize the moment of the hard layer. To test this explanation, we reversed the moment of the free layer by a coherent rotation of its magnetic moment without the formation of domain walls; at 10 Hz, the sample was rotated about its surface, normal in a fixed homogenous magnetic field of 200 Oe, which was applied in the plane of the sample. The magnitude of the fixed field was chosen to be sufficiently larger than the coercivity of the free layer to ensure coherent rotation.

The change in the remanent **M** of the hard layer is shown by a comparison of the results that are obtained by repeatedly rotating a sample with a 50 Å–thick hard layer and by cycling the field on the same sample (Fig. 2). For up to 1.6×10^6 rotations, there is no decay of the hard layer remanent moment within experimental error, whereas the hard layer was completely demagnetized after the same number of cycles. This result clearly shows that the formation and motion of domain walls play an important role in the observed demagnetization process.

The magnitude and spatial extent of the demagnetizing fields from the domain walls in the free layer must depend on the detailed magnetic structure of the domain walls. Thus, it would not be surprising if the **M** decay (which we have observed) depends on the thickness of the hard layer as well as on the composition of the free layer because, for example, the width of the domain wall and, consequently, the strength of the demagnetizing field would also depend on both **M** and the magnetic anisotropy of the free layer. However, it is difficult to probe the domain wall structure. In a magnetic force microscope, the stray field from the magnetic tip disturbs the structure of the magnetically soft free layers in our structures. Instead, we have carried out plan-view Lorentz transmission electron microscopy on structures formed on 500 Å–thick Si_3N_4 membranes. Although some differences are observed between the Co and NiFe layers, it is difficult to resolve the detailed magnetic structure of the domain walls because only the in-plane component of **M** produces contrast. Electron holography will likely provide the additional information that is necessary to understand the details of the domain walls. Further investigations will extend the current study of large-area films to small patterned structures on the scale of domains.

References and Notes

1. J. L. Simonds, *Phys. Today* **48**, 26 (1995); K. G. Ashar, *Magnetic Disk Drive Technology: Heads, Media, Channel, Interfaces, and Integration* (Institute of Electrical and Electronics Engineers, New York, 1997).
2. A. Chiu *et al.*, *IBM J. Res. Dev.* **40**, 283 (1996).
3. G. Binasch, P. Grünberg, F. Saurenbach, W. Zinn, *Phys. Rev. B Condens. Matter* **39**, 4828 (1989); M. N. Baibich *et al.*, *Phys. Rev. Lett.* **61**, 2472 (1988).
4. S. S. P. Parkin, N. More, K. P. Roche, *Phys. Rev. Lett.* **64**, 2304 (1990).
5. B. Dieny *et al.*, *Phys. Rev. B Condens. Matter* **43**, 1297 (1991); S. S. P. Parkin, *Phys. Rev. Lett.* **71**, 1641 (1993); J. C. S. Kools, *IEEE Trans. Magn.* **32**, 3165 (1996); For an explanation and demonstration of the giant MR/spin-valve head, see www.research.ibm.com/research/gmr.html.
6. M. Julliére, *Phys. Lett. A* **54**, 225 (1975).
7. J. S. Moodera, L. R. Kinder, T. M. Wong, R. Meservey, *Phys. Rev. Lett.* **74**, 3273 (1995); S. S. P. Parkin, R. E. Fontana, A. C. Marley, *J. Appl. Phys.* **81**, 5521 (1997); W. J. Gallagher *et al.*, *ibid.*, p. 3741; J. M. Daughton, *ibid.*, p. 3758.
8. A 21% effect is possible with a more complicated spin-valve structure. See W. F. Egelhoff *et al.*, *ibid.* **78**, 273 (1995).
9. J. C. Slonczewski, *Phys. Rev. B Condens. Matter* **39**, 6995 (1989).
10. W. Kayser, *IEEE Trans. Magn.* **3**, 141 (1967).
11. S. S. P. Parkin, R. Bhadra, K. P. Roche, *Phys. Rev. Lett.* **66**, 2152 (1991).
12. L. Néel, *C. R. Hebd. Seances Acad. Sci.* **255**, 1545 (1962); *ibid.*, p. 1676.

13. We thank S. A. Crooker, P. P. Crooker, and M. Scheinfein for helpful discussions. We also thank R. E. Dunin-Borkowski, M. R. McCartney, and D. J. Smith for Lorentz microscopy studies. B.-U.R. thanks the Alexander von Humboldt Foundation, Germany, for a Feodor Lynen Fellowship.

5 December 1997; accepted 26 June 1998

Evidence of Soft-Mode Quantum Phase Transitions in Electron Double Layers

Vittorio Pellegrini, Aron Pinczuk, Brian S. Dennis, Annette S. Plaut, Loren N. Pfeiffer, Ken W. West

Inelastic light scattering by low-energy spin-excitations reveals three distinct configurations of spin of electron double layers in gallium arsenide quantum wells at even-integer quantum Hall states. The transformations among these spin states appear as quantum phase transitions driven by the interplay between Coulomb interactions and Zeeman splittings. One of the transformations correlates with the emergence of a spin-flip intersubband excitation at vanishingly low energy and provides direct evidence of a link between quantum phase transitions and soft collective excitations in a two-dimensional electron system.

A two-dimensional (2D) electron gas, when subjected to a perpendicular magnetic field $B_{\perp}$, exhibits remarkable behavior that follows from the quantization of the in-plane kinetic energy into Landau levels, the Zeeman splitting of different spin states, and the impact of strong Coulomb interactions. The quantum Hall effects occur when changes in $B_{\perp}$ or electron density, or both, cause the Fermi energy to sweep across spin-split Landau levels (*1–3*). Quantum Hall states are distinct phases of the 2D electron gas displaying precise quantization of the Hall effect and vanishing longitudinal magnetoresistance. They are observed at integer and some fractional values of Landau-level filling factor $\nu = n2\pi l_B^2$. Here, n is the areal electron density and $l_B = (hc/2\pi eB_{\perp})^{1/2}$ is the magnetic length. c is the speed of light, h is Planck's constant, and e is the electron charge. Experimental and theoretical studies of quantum Hall phenomena have uncovered some of the more intriguing behavior in contemporary physics. Notable examples are low-temperature quantum phase transitions tuned by the external magnetic field [for recent reviews see (*4–7*)]. Evidence of phase transformations appears in magnetotransport as anomalies in quantum Hall states. In current theories, the transformations are triggered by low-energy collective excitations of quantum Hall states. Within this framework, the softening of a low-energy mode induces an instabilitiy in which the 2D electron system changes quantum ground state by incorporating properties associated with the excitation (*8–12*).

V. Pellegrini, Bell Laboratories, Lucent Technologies, Murray Hill, NJ 07974, USA, and Scuola Normale Superiore and Istituto Nazionale per la Fisica della Materia, Pisa, Italy. A. Pinczuk, Bell Laboratories, Lucent Technologies, Murray Hill, NJ 07974, USA, and Departments of Physics and Applied Physics, Columbia University, New York, NY 10027, USA. B. S. Dennis, L. N. Pfeiffer, K. W. West, Bell Laboratories, Lucent Technologies, Murray Hill, NJ 07974, USA. A. S. Plaut, Department of Physics, University of Exeter, Exeter EX4 4QL, UK.

When the soft mode has vanishingly low energy ($\omega \rightarrow 0$), the spontaneous broken symmetry phase has a continuous order parameter that vanishes at the critical point of the transition.

Continuous quantum phase transitions are remarkable transformations in which quantum mechanical effects dominate physics at temperatures approaching absolute zero. However, even at the lowest accessible temperatures, large thermal populations of low-energy soft modes cause critical fluctuations that destroy the long-range order of the broken symmetry phase (*7*). In 2D systems, short-range order is destroyed in a Kosterlitz-Thouless transition at the critical temperature T_c. Research into such transformations is largely based on studies of scaling behavior of transport data near the critical point. We report studies that enable the direct experimental determination of a link between soft collective modes and a quantum phase transition in a 2D electron system. Soft excitations are measured directly from inelastic light scattering spectra. By giving direct access to the interactions that drive the instability, these studies open up avenues by which to examine these transformations.

Distinct charge or spin collective excitations of quantum Hall states are built from the particle-hole pairs formed by the transitions between energy levels within the 2D electron system (typical spacings are in the millielectronvolt range) (*13*). Electron-electron interactions have a major impact on their wave vector dispersions: the roton (or magnetoroton), a minimum in the dispersion at finite wave vectors $q \approx 1/l_B \approx 10^6$ cm^{-1}, is one of the most notable manifestations of these interactions. Rotons are caused by excitonic terms of the Coulomb interactions, also known as vertex corrections, which bind particle-hole pairs and greatly reduce collective mode energies. Soft ($\omega \rightarrow 0$) rotons are crucially involved in predictions of novel phase transitions tuned by the external magnetic field (*8, 10–12*) and play key roles in the physics of 2D electron systems. Such unstable collective modes, however, have not been observed because the large wave vectors ($q \geq 10^6$ cm^{-1}) and low energies ($\omega \leq 1$ meV) are not easily accessible by current experimental methods.

We studied electron bilayers in double quantum wells. In these structures, tunneling between the two layers determines the splitting Δ_{SAS} of the lowest symmetric and antisymmetric states sketched in Fig. 1A. The electron bilayers are ideal systems to explore the role played by low-energy collective modes in quantum phase transitions because Δ_{SAS} is tunable by the design parameters of the double quantum well. Low-energy tunneling excitations are readily observable by inelastic light-scattering (LS), as demonstrated in our recent measurements of soft spin-excitations at even-integer quantum Hall states (*14, 15*). These are long wavelength ($q \rightarrow 0$) collective excitations of the tunneling gap of GaAs double quantum wells (DQW). Vertex corrections reduce the energies of tunneling spin-excitations to values much lower than Δ_{SAS}, and as a function of the difference ($n_S - n_{AS}$) in the occupation of the symmetric and antisymmetric states, these spin excitations are easily tuned by changes in $B_\perp$. The LS results indicate the existence of unstable $q \rightarrow 0$ spin-flip excitations of vanishingly low energy at Landau-level filling $\nu = 2$ and $n_{AS} = 0$. This work has stimulated calculations that predict a quantum phase transition to a broken symmetry state with canted antiferromagnetic (AF) spin alignment in the two layers (*16, 17*).

Our inelastic LS results uncover evidence that the configurations of the spin of electron double layers do undergo quantum phase transitions that are tunable by magnetic field, and that unstable spin-excitations are involved. We show first that the bilayers at even-integer ν exhibit three distinct phases of spin as a function of two parameters: the total magnetic field B_T and the tunneling gap Δ_{SAS}. To that effect, the tilt angle between B_T and the bilayers (Fig. 2A) is changed while the perpendicular component $B_\perp$ is kept at the chosen value of ν. We find that in one of the phase transitions, a $q \approx 0$ soft spin-excitation mode collapses to vanishingly low energy, thus revealing a connection between the quantum phase transition in the spin degree of freedom and the unstable spin-excitation. A phase diagram describing how the different spin configurations of the even-integer quantum Hall states are tuned by B_T

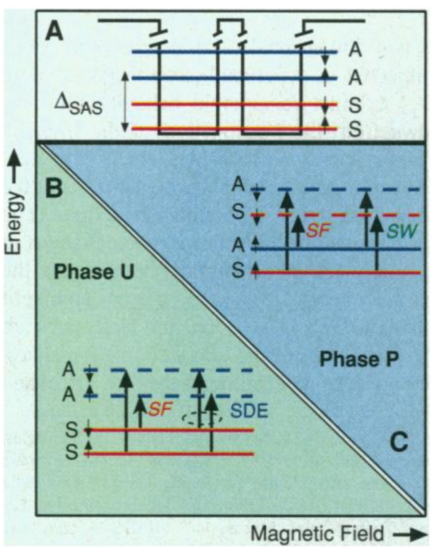

Fig. 1. (**A**) Schematic representation of the potential and energy levels of electrons in the conduction band of a GaAs/AlGaAs double quantum well. Red horizontal lines represent symmetric S states. Antisymmetric A states are represented by blue lines. The short vertical arrows represent the two, up or down, orientations of electron spin in the magnetic field. The tunneling gap Δ_{SAS} is the splitting between symmetric and antisymmetric states with the same orientation of spin. The spin splitting of a state, S or A, is determined by the Zeeman energy E_Z and the spin stiffness due to the increase in Coulomb exchange interaction energy when the spin orientation is changed. (**B**) Schematic representation of the alignment of energy levels of electrons in the spin-unpolarized phase U at $\nu = 2$. Solid lines correspond to occupied levels and dashed lines are empty levels. Vertical arrows labeled *SF* indicate the transitions that contribute to spin-flip tunneling excitations. The spin-density tunneling excitations are constructed with linear combinations of the two transitions labeled *SDE* (*15*). (**C**) Schematic representation of the alignment of energy levels in the spin-polarized phase P at $\nu = 2$. Vertical arrows labeled *SF* indicate the transitions that contribute to spin-flip tunneling modes. The transitions that contribute to spin-wave modes, in which there is only change in the orientation of spin, are indicated by vertical arrows labeled *SW*.

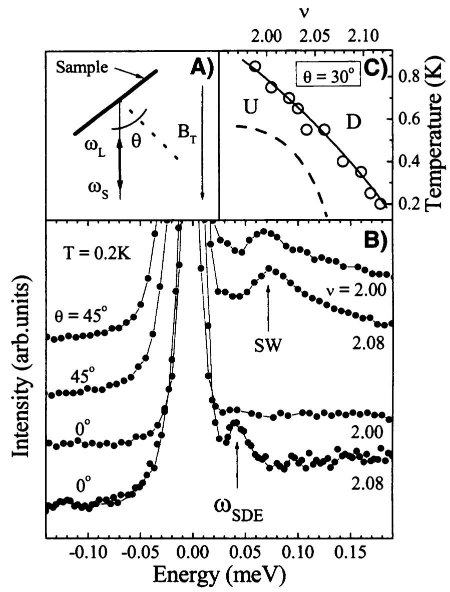

Fig. 2. (**A**) Sketch of the tilted field geometry adopted in the experiment. ω_L and ω_S are energies of the incident (laser) and scattered light. B_T is the total magnetic field and θ the tilt angle. (**B**) Resonant inelastic light scattering spectra with orthogonal linearly polarized incident and scattered light for the GaAs quantum well sample with $n = 9.96 \times 10^{10}$ cm^{-2} and $\Delta_{SAS} = 0.6$ meV. At $\theta = 0°$ and $\nu = 2.08$, the peak corresponds to the $\delta S_z = 0$ SDE mode. At $\theta = 45°$, the peaks correspond to spin wave across the Zeeman gap. (**C**) The circles show the dependence of T_c versus filling factor at $\theta = 30°$ (T_c is the lowest value of the temperature at which the SDE modes reappear in the spectra of phase D). The dashed line is T_c measured at $\theta = 0°$ [after (*14*)].

displays two phase boundaries that separate the three spin configurations. The predictions of (*17*) are in qualitative agreement with this construction.

Two possible configurations of spin have been proposed for electron double layers at even-integer values of ν, shown schematically (Fig. 1, B and C) for the case of $\nu = 2$. Phase U (Fig. 1B) is spin-unpolarized. Phase P (Fig. 1C) is spin-polarized [ferromagnetic (FM)]. The actual spin configuration will depend on the strength of the energy required to produce a spin-flip relative to that of the interlayer interactions that enter in the tunneling gap Δ_{SAS}. The energy required to change the orientation of spin incorporates two terms. One is the Zeeman energy $E_Z = g\mu_B B_T$, where g is the gyromagnetic ratio and μ_B is the Bohr magneton. The other is the spin stiffness of the 2D electron system, given by the increase in Coulomb exchange interaction energy when the spin orientation is changed. Because the spin stiffness has a characteristic $(B_\perp)^{1/2}$-dependence (*4, 13, 17, 18*), phase U prevails at the lower values of $B_\perp$ and B_T (*14, 15*). Phase P emerges at higher fields when the spin-flip transition energy in the lowest Landau level is larger than the energy associated with a transition across the tunneling gap (*19*). The soft modes occur in phase U, and the LS spectra reveal that this phase evolves into a third, disordered spin state we call phase D (*15*).

Phases U and P have very different spin-excitations classified by δS_z, the change in spin angular momentum along B_T. The tunneling modes of phase U have been considered in (*15*). Here, spin-excitations are triplets at energies $\omega = \omega_{SDE} - E_Z\delta S_z$, where $\delta S_z = 0, \pm 1$ and ω_{SDE} is the energy of the spin-density excitation (SDE) with $\delta S_z = 0$. The two transitions that contribute to SDE modes are shown in Fig. 1B, which also shows the transitions of tunneling spin-flip (SF) mode with $\delta S_z = \pm 1$. The emergence of phase P is characterized by spin-wave (SW) modes associated with the two $\delta S_z = -1$ SW transitions shown in Fig. 1C. The SW energy *in the limit $q \rightarrow 0$ is set at E_Z by Larmor's* theorem (*13*). The two phases are thus identifiable from LS spectra. Phase U has well-defined SDE excitations as previously reported (*15*), and the signature of phase P is the appearance of long-wavelength SW excitations.

The experiments were carried out in DQW samples that consisted of two nominally identical, 180 Å–thick GaAs quantum wells separated by an $Al_{0.1}Ga_{0.9}As$ undoped barrier of 79 Å width. Free electron concentrations were between $n = 6.2 \times 10^{10}$ cm^{-2} and 1.44×10^{11} cm^{-2}, and low-temperature mobilities were close to 10^6 cm^2 V^{-1} s^{-1}. At $B_T = 0$, tunneling gaps are $\Delta_{SAS} < 0.7$ meV (*20*). Resonant inelastic LS was studied in the geometry shown in Fig. 2A using a diode laser tuned near the fundamental optical transitions of the GaAs DQW (close to 812 nm). Crossed light polarizations for incident and scattered photons were used to detect inelastic LS from spin-excitations. We are interested here in tunneling excitations and also in SW modes. For $\theta = 0$, tunneling modes with $\delta S_z = 0$ are allowed (*15*). For $\theta \neq 0$, spin-waves with $\delta S_z = \pm 1$ also become allowed because of the non-zero component of the light polarization along the magnetic field B_T axis (*21*). Incident power densities were kept below 10^{-4} W/cm^2, and spectra were recorded with multichannel detection at a spectral resolution of 0.02 meV. The samples were mounted in a ^{3}He/^{4}He dilution refrigerator with optical windows. Accessible temperatures are in the range $0.2\ \mathrm{K} \leq T \leq 2$ K.

To show the impact of changes in B_T at constant ν, characteristic spectra from the three phases of spin at $\nu \approx 2$ are shown (Fig. 2B). The results for $\theta = 0$ ($B_T = B_\perp$) are similar to those previously reported (*15*). At $\nu = 2.08$, we found the well-defined peak of SDE at ω_{SDE}. The abrupt disappearance of this mode at $\nu = 2.00$ is taken as indication *that a new spin configuration has emerged,* and the absence of an LS signal suggests a disordered state D. This transition occurs when $\omega_{SDE} \rightarrow E_Z$, implying the existence of a $\delta S_z = 1$ SF tunneling excitation at vanishingly small energy $\omega_{SDE} - \delta S_z E_Z$ (*15*).

Figures 2B and 3 display drastically different behavior at $\theta = 45°$ where collective spin-excitations reappear in the spectra, and the modes can now be measured over a very broad range of B_T and filling factor. Particularly revealing is the evidence in Fig. 3 that at $\theta = 45°$, the spin-excitation modes near $\nu = 2$ blend smoothly with the SW excitations across the Zeeman gap at energies E_Z. Such behavior indicates that at $\theta = 45°$, only SW excitations are observed for $\nu \geq 2$ and that these excitations have replaced in the LS spectra the SDE modes seen at $\theta = 0°$. Because the presence of spin-wave excitations is the characteristic signature of the spin-polarized state, Figs. 2B and 3 offer direct evidence that when $\theta = 45°$, phase P emerges at filling factors $\nu \approx 2$.

The results in Fig. 4 show the very distinct field dependences of the excitations measured for different tilt angles. The main characteristic of SDE modes seen in phase U is their softening with B_T and their disappearance when reaching E_Z at $\nu \approx 2$. These changes are indeed observed for $\theta \leq 30°$ and fields $B_T \leq 2.4T$. Spin-waves appear in the LS spectra of this sample for larger tilts and fields $B_T > 2.4T$. Figures 3 and 4 thus demonstrate the identification of phase P by inelastic LS. The SW mode energies of phase P, however, display an unexpected blueshift from E_Z for $\nu \approx 2$ and broader spectral linewidth. At this time, we do not have an explanation for such behavior. One intriguing scenario is that at this field there is disorder and loss of rotational invariance that remove the restrictions imposed by Larmor's theorem.

The results in Figs. 2B through 4 offer the crucial evidence that links the soft spin-excitations of phase U to a quantum phase transition in the spin degree of freedom at $\nu \approx 2$. They reveal that the three possible configurations of spin of the electron double layers are accessed by changing the total field B_T while keeping $B_\perp$ at values of $\nu \approx 2$. U and P are well-defined phases with the configurations sketched in Fig. 1. The disordered state D has a similar pronounced sensitivity on B_T, implying it has to be regarded as a distinct phase of spin. Phase D emerges at the fields where the energy of the SDE mode of phase U is $\omega_{SDE} \rightarrow E_Z$. Thus, the $U \rightarrow D$ transformation is a quantum phase transition, tuned by B_T, that

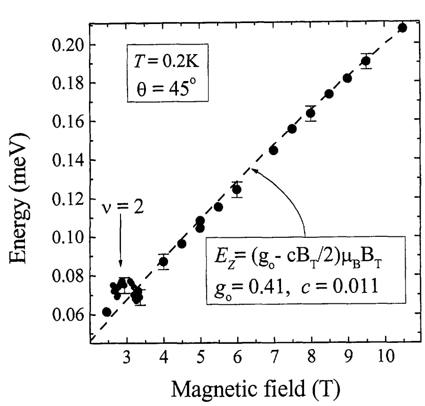

Fig. 3. Energies of spin-excitations as a function of total magnetic field at $\theta = 45°$. The line through the data is a fit to the equation $E_Z = (g_o - cB_T/2)\mu_B B_T$. The modes are thus identified with long wavelength ($q \rightarrow 0$) SW excitations.

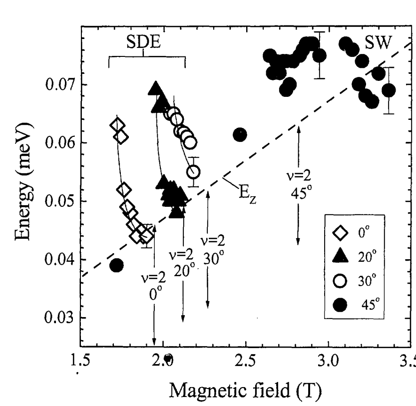

Fig. 4. Energies of spin-excitation modes as function of total magnetic field measured at tilt angles (θ) between 0° and 45°. Vertical lines indicate the B_T values of $\nu = 2$ for the tilt angles of the experiments. The dotted line is the E_Z shown in Fig. 3.

correlates with the emergence of a soft spin-flip ($\delta S_z = 1$) mode of vanishingly low energy close to $\omega_{SDE} - E_Z$.

The inelastic LS results also enable the construction of a spin-configuration phase diagram at filling factors $\nu = 6$ and $\nu = 2$. Figure 5 shows the diagram obtained from data measured in four DQW samples that differ in density and Δ_{SAS}. The diagram confirms that at large B_T and relatively small Δ_{SAS}, the bilayers are in the spin-polarized phase P. At smaller magnetic fields such that $\Delta_{SAS} \gg E_Z$, the bilayers are in the spin-unpolarized phase U. The new phase D occurs at intermediate Δ_{SAS} and E_Z, when the $q \approx 0$ tunneling spin-excitation becomes soft. The phase diagram in Fig. 5 is consistent with the predictions of (17). The soft-mode having $\delta S_z = +1$ suggests an order-parameter associated with the operator $\delta S^+ = \delta(S_x - iS_y)$. Such broken-symmetry is consistent with a canted AF phase, as proposed in (16, 17).

The LS spectra of phase D have an intriguing T dependence in which SDE excitations at $\nu = 2$ reappear for $T \geq 0.5$ K (15). This unexpected behavior is evidence of a reversal $D \rightarrow U$ transformation at a temperature $T_c \cong 0.5$ K. We have studied this effect as a function of tilt angle. Figure 2C shows T_c measured at 30° (solid circles). Comparison with the 0° results (dashed line) reveals an enhanced stability of phase D at finite tilt. From LS spectra obtained at $\nu \simeq 6$ we determined that changing the tilt angle from 0° to 30° reduces Δ_{SAS} by about 0.05 meV, as predicted by current theory (22). Thus, the results in Fig. 2B indicate that the increased stability of phase D correlates with a reduction in Δ_{SAS}. This behavior is consistent with the proposal that phase D is a Kosterlitz-Thouless state with a transition temperature T_c (17).

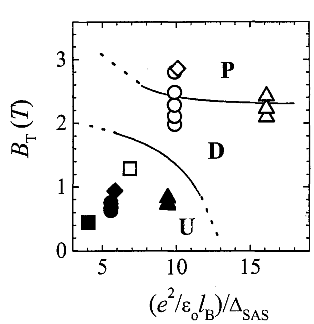

Fig. 5. Phase diagram of electron bilayers at even values of ν and $T = 0.2$ K. The total magnetic field B_T is plotted here against the reciprocal tunneling gap in units of the Coulomb interaction energy $(e^2/\epsilon_o l_B)$, where ϵ_o is the dielectric constant. Solid lines indicate the positions of the phase boundaries determined from experiment. Dotted lines are introduced to give continuity to the boundaries. The samples are GaAs quantum wells of different densities. Squares, $n = 6.2 \times 10^{10}$ cm^{-2}; circles, $n = 9.9 \times 10^{10}$ cm^{-2}; triangles, $n = 1.05 \times 10^{11}$ cm^{-2}; and diamonds, $n = 1.44 \times 10^{11}$ cm^{-2}. Open symbols are for $\nu = 2$ and closed symbols for $\nu = 6$.

Finally, measurements of SW modes yield precise determinations of E_Z over a wide range of B_T. To this effect, we carried out a fit by means of the expression $E_Z = (g_o - cB/2)\mu_B B$, which incorporates a small quadratic correction to the g factor (23). The best fit is shown as dotted lines in Figs. 3 and 4. These determinations enable the evaluation of the Zeeman energy at field close to $\nu = 2$. We find in Fig. 4 that the energy of the SDE tunneling mode reaches the value $\omega_{SDE} = E_Z$ when the SDE peak disappears with the emergence of phase D. This result is a strong indication that the $U \rightarrow D$ transition might be continuous. Experiments carried out at lower temperatures could offer further insights. The instability could also be investigated by activated magnetotransport (24).

References and Notes

1. R. E. Prange and S. M. Girvin, Eds., *The Quantum Hall Effect* (Springer, New York, ed. 2, 1990).
2. T. Chakraborty and P. Pietilainen, *The Quantum Hall Effects: Integral and Fractional*, vol. 85 of the Springer Series in Solid State Sciences (Springer, New York, ed. 2, 1995).
3. S. Das Sarma and A. Pinczuk, Eds., *Perspectives in Quantum Hall Effects* (Wiley, New York, 1996).
4. K. Moon *et al.*, *Phys. Rev. B* **51**, 5138 (1995).
5. J. P. Eisenstein, in (3), pp. 37–70.
6. M. Shayegan, *ibid.*, pp. 343–384.
7. S. L. Sondhi *et al.*, *Rev. Mod. Phys.* **69**, 315 (1997).
8. S. M. Girvin, A. H. MacDonald, P. M. Platzman, *Phys. Rev. B* **33**, 2481 (1985).
9. H. A. Fertig, *ibid.* **40**, 1087 (1989).
10. A. H. MacDonald, P. M. Platzman, G. S. Boebinger, *Phys. Rev. Lett.* **65**, 775 (1990).
11. L. Brey, *ibid.*, p. 903.
12. R. K. Kamilla and J. K. Jain, *Phys. Rev. B* **55**, R13417 (1997).
13. C. Kallin and B. I. Halperin, *ibid.* **30**, 5655 (1984).
14. A. Pinczuk *et al.*, *Bull. Am. Phys. Soc.* **41**, 482 (1996); A. S. Plaut, *ibid.*, p. 590.
15. V. Pellegrini *et al.*, *Phys. Rev. Lett.* **78**, 310 (1997).
16. L. Zheng *et al.*, *ibid.*, p. 2453.
17. S. Das Sarma *et al.*, *ibid.* **79**, 917 (1997).
18. G. F. Giuliani and J. J. Quinn, *Phys. Rev. B* **31**, 6228 (1985).
19. G. S. Boebinger, H. W. Jiang, L. N. Pfeiffer, K. W. West, *Phys. Rev. Lett.* **64**, 1793 (1990).
20. A. S. Plaut *et al.*, *Phys. Rev. B* **55**, 9282 (1997).
21. Y. Yafet, *Phys. Rev.* **152**, 858 (1966). For the same reason, the tilted field geometry allows inelastic light scattering from spin-flip intersubband modes with $\delta S_z = \pm 1$. We have found, however, little evidence of such modes in the resonant inelastic light scattering spectra at ν close to 2. This may stem from the presence of several relaxation channels for the intersubband spin-flip modes and the consequent broadening of the peak.
22. J. Hu and A. H. MacDonald, *Phys. Rev. B* **46**, 12554 (1992).
23. M. Dobers, K. v. Klitzing, G. Weiman, *ibid.* **38**, 5453 (1988); M. J. Snelling *et al.*, *ibid.* **44**, 11345 (1991).
24. A. Sawada *et al.*, *Phys. Rev. Lett.* **80**, 4534 (1998).
25. We thank K. W. Baldwin for magnetotransport measurements.

7 April 1998; accepted 23 June 1998

Preparation of Photonic Crystals Made of Air Spheres in Titania

Judith E. G. J. Wijnhoven and Willem L. Vos*

Three-dimensional crystals of air spheres in titania (TiO_2) with radii between 120 and 1000 nanometers were made by filling the voids in artificial opals by precipitation from a liquid-phase chemical reaction and subsequently removing the original opal material by calcination. These macroporous materials are a new class of photonic band gap crystals for the optical spectrum. Scanning electron microscopy, Raman spectroscopy, and optical microscopy confirm the quality of the samples, and optical reflectivity demonstrates that the crystals are strongly photonic and near that needed to exhibit band gap behavior.

There is currently an intensive effort to develop porous materials with a wide range of pore sizes up to 30 nm that open up new opportunities in catalysis and separation technology (1, 2). These materials are made by using self-organizing systems, such as surfactant liquids and biological systems as templates for the deposition of inorganic materials. An emerging field that benefits from crystalline macroporous materials (3) is the field of photonic crystals, that is, three-dimensional (3D) dielectric composites with lattice spacings of the order of wavelengths of light (about 500 nm) (4). These crystals can be used to create photonic band gaps (frequency ranges that will not propagate light because of multiple Bragg reflections) (5) that induce useful optical properties, such as inhibition of spontaneous emission or photon localization (4). To achieve band gaps for the visible and infrared spectrum, several challenges exist: both constituent materials of the crystal should be topologically interconnected (6) and the ratio of their refractive indices n should at least be 2 (5). We have synthesized crystals of air spheres in titania that meet these criteria. In

Van der Waals-Zeeman Instituut, Universiteit van Amsterdam, Valckenierstraat 65, NL-1018 XE Amsterdam, Netherlands. http://www.wins.uva.nl/research/scm

*To whom correspondence should be addressed. E-mail: wvos@phys.uva.nl